Hindawi
International Journal of Polymer Science
Volume 2019, Article ID 3864835, 17 pages
https://doi.org/10.1155/2019/3864835

Research Article

Electrophoretic Deposition of Chitosan Films Doped with $Nd_2Ti_2O_7$ Nanoparticles as Protective Coatings against Corrosion in Saline Solutions

M. Martinez-Gomez,[1,2] A. Quinto-Hernandez,[2] N. S. Flores-Garcia,[1] Jan Mayén,[3] M. Dominguez-Diaz,[1] H. Martinez,[1] J. Porcayo-Calderon,[4] J. G. Gonzalez-Rodriguez,[4] and L. Martinez-Gomez[1,5]

[1]*Instituto de Ciencias Físicas, Universidad Nacional Autónoma de México, Avenida Universidad s/n, 62210 Cuernavaca, MOR, Mexico*
[2]*Tecnológico Nacional de México-Instituto Tecnológico de Zacatepec, Calzada Instituto Tecnológico 27, 62780 Zacatepec, MOR, Mexico*
[3]*CIATEQ A.C., Eje 126 No. 225, Zona Industrial, San Luis Potosí, SLP C.P. 78395, Mexico*
[4]*CIICAp, Universidad Autónoma del Estado de Morelos, Avenida Universidad 1001, 62209 Cuernavaca, MOR, Mexico*
[5]*Corrosion y Protección (CyP), Buffon 46, 11590 Mexico City, Mexico*

Correspondence should be addressed to J. Porcayo-Calderon; jporcayoc@gmail.com

Received 24 August 2018; Revised 8 December 2018; Accepted 9 January 2019; Published 17 March 2019

Academic Editor: Marta Fernández-García

In this study, the electrophoretic deposition of chitosan films doped with $Nd_2Ti_2O_7$ nanoparticles was carried out as corrosion protection systems for exposed materials in aqueous environments rich in chlorides. Completely crystalline $Nd_2Ti_2O_7$ nanoparticles with an average size of 100-200 nm were obtained. Electrophoretic deposition of chitosan films with $Nd_2Ti_2O_7$ nanoparticles was possible. With a working voltage of 5 V and 20 minutes of deposition, homogenous chitosan films with a thickness of 4 microns were obtained. According to the FT-IR (Fourier transform infrared spectroscopy), Raman, and XRD (X-ray diffraction) analyses, it was observed that the presence of the nanoparticles modified the properties of the chitosan films, that is, their crystallinity was increased and their moisture absorption capacity was reduced. These modifications caused a better performance against the corrosion of chitosan films deposited on 1018 carbon steel. Its electrochemical evaluation showed that the chitosan films perform as cathodic coatings by affecting the oxygen reduction reaction. This was possible due to the barrier effect of the $Nd_2Ti_2O_7$ nanoparticles, by blocking the effective area for the diffusion of the aggressive electrolyte species.

1. Introduction

It is known that the main objective of organic coatings as protective systems against corrosion is to prevent or mitigate the attack of the substrate by the aggressive anions present in the electrolyte [1, 2]. Due to this, the integrity of the coating used as a protective system against corrosion is fundamental. One way to achieve this goal is to strengthen the structure of the protective film by using healing agents, crosslinking agents, and incorporation of corrosion inhibitors or inert particles that block the diffusion of aggressive anions and also improve the adhesion of the coating towards the substrate [1–11].

Today, protective systems based on environmentally friendly coatings have found great interest in the scientific community. In this sense, due to its excellent properties such as biocompatibility, antimicrobial activity, biodegradability, and its ability to form stable films, chitosan emerges as an alternative for both the formulation and development of protective films that reduce the degradation of materials [4, 5]. In general, chitosan is the result of the deacetylation of chitin and is a compound of low toxicity and is biodegradable and

insoluble in water; its solubility is possible in diluted aqueous solutions due to the protonation of its amine group [3, 12]. Its applications are very diverse and range from medicine, articles for beauty (cosmetics), and the food industry among others.

Chitosan films are natural organic polymers with high chelating capacity towards metal surfaces due to the high charge density existing in the polymer ion which leads to chelation with the metal ion. The presence of both amino and hydroxyl groups in the molecular structure of chitosan is responsible for the ionic interactions with a metal surface [12–15].

The improvement of the protective properties of organic coatings can be achieved through either incorporation or codeposition of nanometric fillers which can enhance their barrier properties [3]. The chitosan can be easily dissolved in dilute acetic acid, and during the dissolution process, its amine groups are protonated resulting in a polyelectrolyte-type solution [5, 16–18]. It is for this reason that chitosan films can be easily deposited by simply applying it in solution on a metal surface and removing its moisture by evaporation.

However, it has been found that electrophoretic deposition of chitosan yields films with better protective properties [6, 18]. During the electrophoretic deposition process, macromolecules with high density of positive charge such as chitosan (due to its amine groups) move toward a substrate (cathode) under the influence of an electric field and are precipitated on its surface [18–20]. The precipitation of the chitosan films is due to the neutralization of their protonated groups by the charge transfer of the OH anions generated electrochemically on the cathode surface [20].

However, because chitosan coatings have a high water absorption capacity, this limits their protective capacity against corrosion. That is why in this study the barrier properties of the chitosan films are increased by the codeposition of neodymium titanate nanoparticles ($Nd_2Ti_2O_7$), where the high activity of its functional groups (amine and OH) will favor the codeposition of the nanoparticles. $Nd_2Ti_2O_7$ is a perovskite-type oxide with high chemical resistance and stable at elevated temperatures; in addition, due to its high concentration of anions and cations, this type of mixed oxides possesses a high density of active sites available to interact with chitosan functional groups. That is why its codeposition can help to increase the protective capacity against corrosion of chitosan films. The chitosan films were deposited by electrophoretic deposition on 1018 carbon steel substrates, and their protective capacity against corrosion was evaluated by electrochemical techniques in a saline solution at room temperature.

2. Experimental Procedure

2.1. Synthesis of the Nanoparticles. Figure 1 details the process for obtaining the precursor gel of the $Nd_2Ti_2O_7$ nanoparticles. Due to the high reactivity of titanium tetraisopropoxide (TTIP), in this process, no water was used for the synthesis of the precursor gel of the nanoparticles; a similar process has been reported in the literature [21].

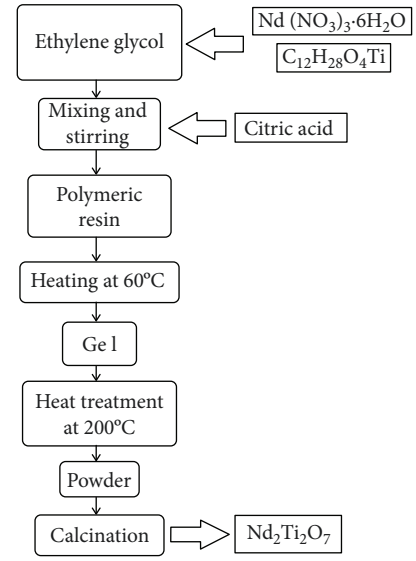

Figure 1: Scheme of the synthesis of $Nd_2Ti_2O_7$ nanoparticles.

The synthesis process was carried out in the following way: 2 moles of ethylene glycol ($C_2H_6O_2$) was added and 0.4 moles of TTIP ($C_{12}H_{28}O_4Ti$) was added; until its complete dissolution assisted by magnetic stirring, subsequently, 0.4 moles of neodymium nitrate ($Nd[NO_3]_3{\cdot}6H_2O$) was added. The mixture was held under stirring for 2 hours. Subsequently, 0.8 moles of anhydrous citric acid ($C_6H_8O_7$) was added until completely dissolved. The polymer resin obtained was stirred for 12 hours at 60°C to promote the polymerization and slow removal of solvents until a highly viscous transparent solution was obtained. The gel was characterized by thermogravimetry and differential thermal analysis (TG/DTA). The gel was transferred to a quartz crucible and subjected to a precalcination treatment in an electric oven for 2 hours at 200°C and finally calcined at 1000°C for 24 hours in static air (this condition was established based on the TGA-DTA analysis). The compound obtained after calcination was characterized by XRD and scanning electron microscopy (SEM).

2.2. Electrophoretic Deposition. 1018 carbon steel samples ($10 * 10$ mm) were used as a cathode and a graphite rod (diameter 4 cm) was used as an anode. The anode-cathode separation was 10 mm. The carbon steel samples were subjected to a process of roughing their surface with abrasive paper from grain 120 to grain 600, and later they were washed with distilled water and ethanol and used immediately in the deposition process. To prepare the chitosan solutions, chitosan with a degree of deacetylation of 85% and molecular weight less than 190 kDa was used. The chitosan was dissolved in a 1% acetic acid solution with constant stirring for 24 hours. In the case of chitosan solutions with nanoparticles, these were added to the chitosan solution, allowing their dispersion with constant agitation for 24 hours and then the solution was left to rest for 24 hours before being used in the electrophoretic deposition process. The electrophoretic deposition of the chitosan films was done using an ethanol-chitosan solution mixture, where the

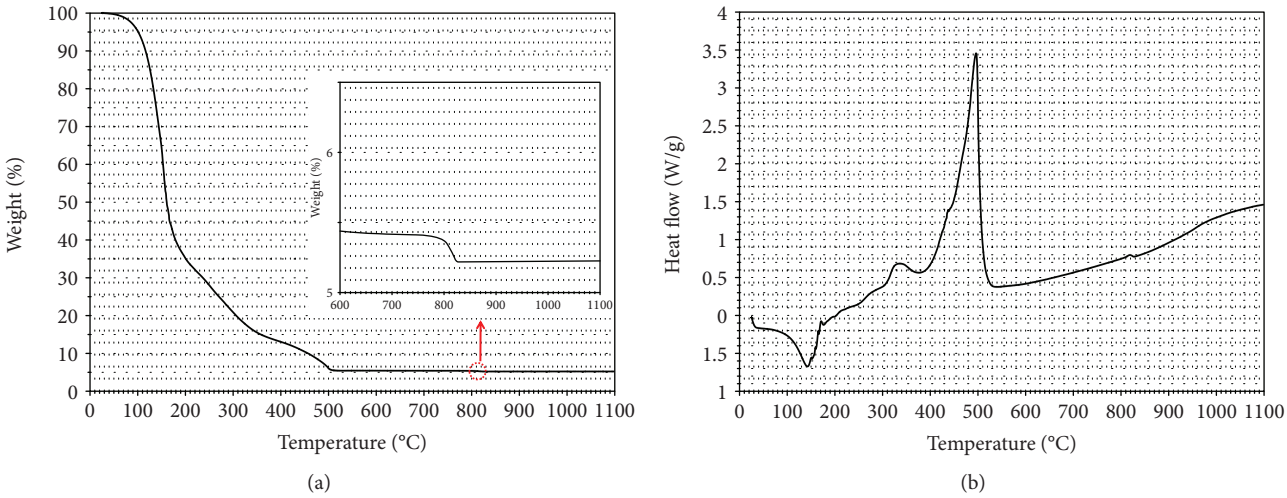

Figure 2: TGA-DTA analysis of the nanoparticle precursor gel (heating rate 5°C/min in air).

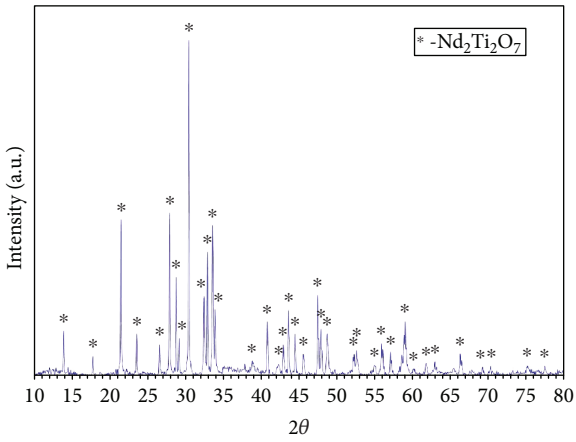

Figure 3: XRD pattern of the $Nd_2Ti_2O_7$ nanoparticles.

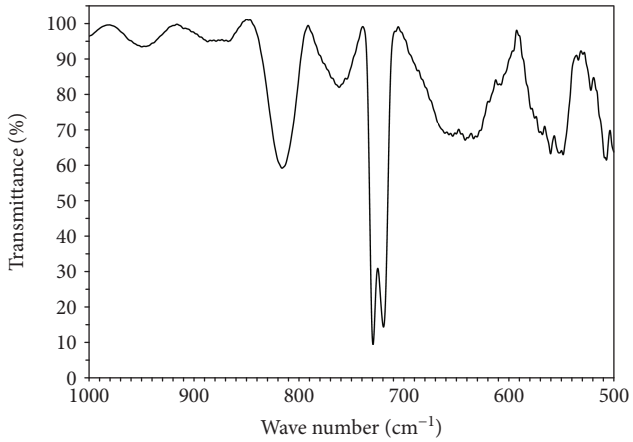

Figure 4: FT-IR spectrum of the $Nd_2Ti_2O_7$ nanoparticles.

percentage of chitosan solution was 17% (*v*/*v*). The chitosan solution was prepared by dissolving 0.5 grams of chitosan in one liter of 1% (*v*/*v*) acetic acid solution. Based on previous tests, it was established to carry out the film deposition by applying a voltage of 5 V at different deposition times. Higher concentrations of chitosan, as well as larger deposition voltages, provoke surface defects due to the accumulation of H_2.

Under these deposition conditions, chitosan films doped with nanoparticles were deposited at different concentrations (0, 100, 500, and 1000 ppm). In all cases, once the chitosan films were deposited, they were allowed to dry at room temperature for 24 hours before any subsequent analysis or use. The films deposited were characterized by FT-IR, Raman, DRX, and SEM.

2.3. Electrochemical Evaluation of Chitosan Films. The deposited chitosan films were evaluated in their state as deposited without any additional treatment. As a corrosive medium, a 3.5% (by weight) NaCl solution was used at room temperature under nonaerated conditions.

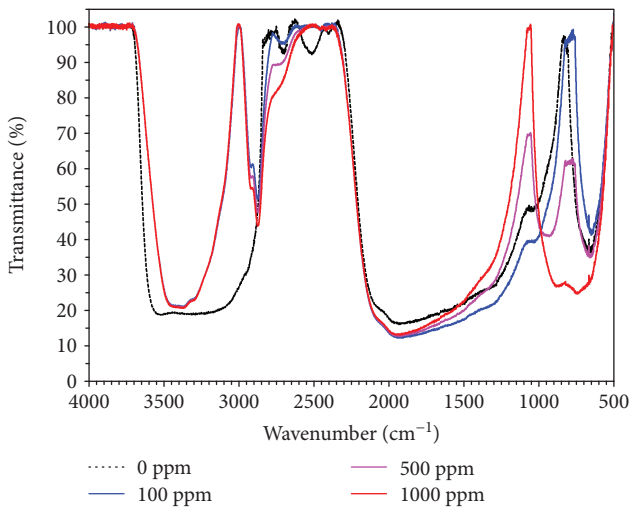

Figure 5: FT-IR spectra of chitosan films doped with nanoparticles.

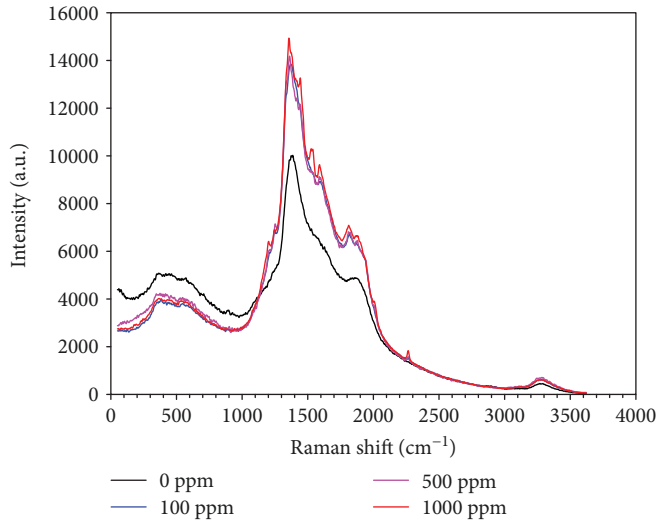

Figure 6: Evolution of the Raman spectra of doped chitosan films with different concentrations of nanoparticles.

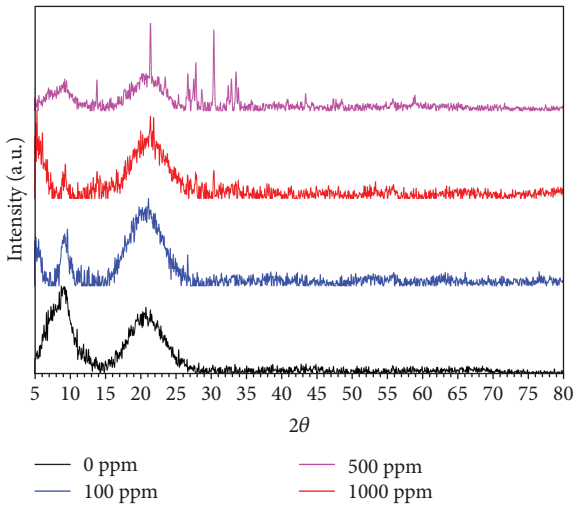

Figure 7: DRX pattern of chitosan films doped with $Nd_2Ti_2O_7$ nanoparticles.

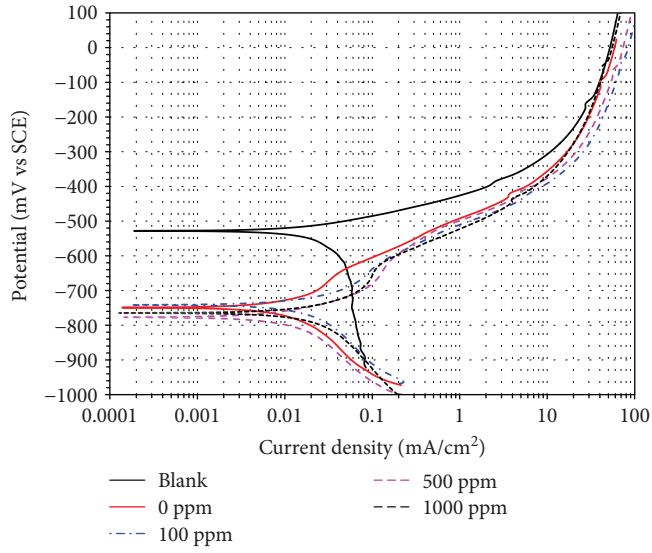

Figure 8: Polarization curves for 1018 carbon steel bare and coated with chitosan doped with nanoparticles.

The electrochemical evaluation was carried out in a three-electrode electrochemical cell using the samples coated with the chitosan films as working electrodes, a saturated calomel electrode as a reference electrode, and a graphite bar, with an area greater than that of the working electrode, as counter-electrode. The electrochemical techniques used were potentiodynamic polarization curves, open circuit potential (OCP) measurements, linear polarization resistance (LPR) measurements, and electrochemical impedance spectroscopy (EIS).

Potentiodynamic polarization curves were obtained by polarizing the working electrode from -400 to 1000 mV with respect to its corrosion potential at a scanning rate of 1 mV/s. OCP measurements were carried out by recording the potential of the working electrode with respect to the reference electrode at one hour intervals. For LPR measurements, the working electrode was polarized ±10 mV with respect to its open circuit potential at a speed of 0.1667 mV/s, and the value of the polarization resistance (R_p) was determined from the slope of the ratio current potential obtained. The measurements were made at one hour intervals. EIS spectra were obtained by applying an amplitude perturbation of 10 mV with respect to the open circuit potential of the working electrode in a frequency range of 100 kHz to 0.01 Hz.

OCP, LPR, and EIS measurements were performed for 24 hours. In all cases, before starting any measurement, the electrochemical cell was allowed to stabilize for 15 minutes. The potentiodynamic polarization curves were obtained with a Gill AC potentiostat/galvanostat from ACM Instruments and the OCP, LPR, and EIS measurements in an Interphase 1000 potentiostat/galvanostat/ZRA analyzer from Gamry.

Table 1: Electrochemical parameters from polarization curves.

1018 carbon steel	E_{corr} (mV)	βa (mV/Dec)	-βc (mV/Dec)	I_{corr} (μA/cm^2)
Bare	-529 (±5)	71 (±5)	748 (±5)	36.5 (±3)
Chitosan coating (0 ppm)	-749 (±3)	215 (±6)	245 (±4)	14.1 (±2)
Chitosan coating(100 ppm)	-743 (±3)	141 (±5)	230 (±3)	18.8 (±2)
Chitosan coating (500 ppm)	-778 (±4)	106 (±3)	219 (±5)	13.6 (±1)
Chitosan coating (1000 ppm)	-765 (±4)	111 (±4)	191 (±5)	19.0 (±1)

3. Results and Discussion

3.1. Synthesis of $Nd_2Ti_2O_7$ Nanoparticles. Figure 2 shows the thermal behavior of the precursor gel of $Nd_2Ti_2O_7$ nanoparticles. It is known that during the thermal treatment of the gel, both the nitrates and the complexing elements (citric acid) and gelling agents (ethylene glycol) behave as "oxidants" and "fuels" which produce the "ashes" containing the desired compound. Exothermic processes are associated with the decomposition of nitrates and the oxidation of organic compounds. The release of gases (NO_2, H_2O, and CO_2) favors the product disaggregation, increasing its porosity and the dissipation of heat, inhibiting its sintering, and forming very fine particles [22].

From the TGA-DTA curves, the occurrence of three main decomposition events can be observed from room temperature to 530°C. The first of these is an endothermic event at 140°C associated with a mass loss of approximately 60%. This event corresponds to the greatest loss of mass and can be attributed mainly to the decomposition of ethylene glycol present in excess and to the dehydration of moisture tightly bound to the complexes [23]. The second one is an exothermic event at 330°C associated with an additional mass loss of approximately 25%. This event can be associated with the separation of the ethylene glycol bound as an adduct and as an ester, in addition to the decarboxylation of the COOH groups (existing or formed as a result of the deesterification) [23]. The third one is the main exothermic event at 495°C associated with an additional mass loss of approximately 10%. This event can be associated to the pyrolysis and combustion of the organic skeleton where one of the reaction products is residual carbon and amorphous oxycarbonates of the bimetallic system (possibly $Nd_2Ti_2O_5(CO_3)_2$) [23]. It is indicated that due to the formation of these intermediate compounds, higher temperatures are required to obtain the final product [23–25]. Generally, these large exothermic peaks overlap endothermic processes such as decomposition of carboxylic groups, carbonates, and nitrates [26]. Despite the presence of these main events, it is possible to distinguish a small exothermic event at 815°C associated with a small mass loss of 0.2%. This event has been associated with the decomposition of mixed oxycarbonates that give rise to the desired final product [21, 23, 25].

Based on this analysis and in order to guarantee the complete elimination of intermediate reaction products and the crystallinity of the nanoparticles, a calcination temperature of 1000°C was chosen for the $Nd_2Ti_2O_7$ synthesis. Similar temperature conditions have been reported in the literature for rare earth titanates [22].

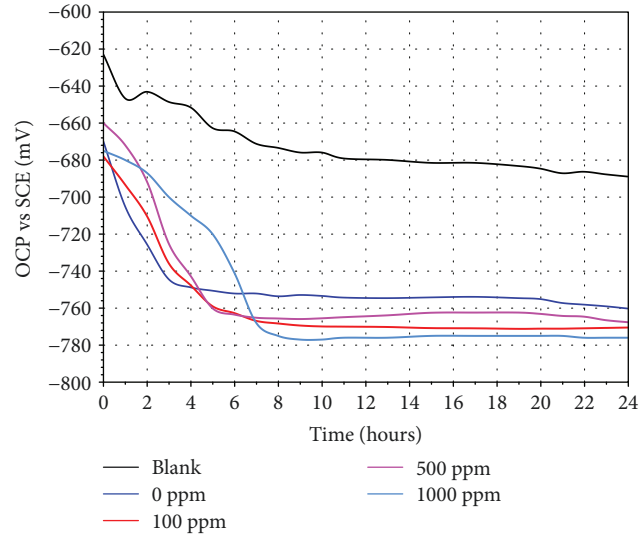

Figure 9: OCP values for 1018 carbon steel bare and coated with chitosan doped with nanoparticles.

Figure 3 shows the X-ray diffraction pattern of the neodymium titanate synthesized after heat treatment of the precursor gel in air at 1000°C for 24 hours. According to the spectrum, it can be confirmed that all the peaks are attributed to the $Nd_2Ti_2O_7$ phase, confirming the excellent crystallinity of the nanoparticles [21, 27, 28].

It should be noted that, if the stoichiometry is not respected (due to the hydrolysis of titanium isopropoxide), the appearance of peaks attributed to TiO and Nd_2O_3, in addition to the $Nd_2Ti_2O_7$ lines, would be observed. The peaks show a unique orientation (00l). The interreticular distances d_{00l} coincide with the reference data JCPDS #33-0942 corresponding to the $Nd_2Ti_2O_7$ monoclinic [28, 29]. It has been reported that $Nd_2Ti_2O_7$ has a thermodynamically stable stratified perovskite structure [30].

Figure 4 shows the FT-IR spectrum of the $Nd_2Ti_2O_7$ nanoparticles. The spectrum shows the main spectral bands corresponding to the different vibrations Ti-O and Nd-O in the frequency region of interest 500-1000 cm^{-1}. The stretching vibrations of the Ti-O bond are located in the regions of 1087-695 and 625-310 cm^{-1}, and the band around 760 cm^{-1} corresponds to the TiO_4 tetrahedron, and the stretching vibrations of the Nd-O bond are located around 644 cm^{-1} and 510 cm^{-1} [31].

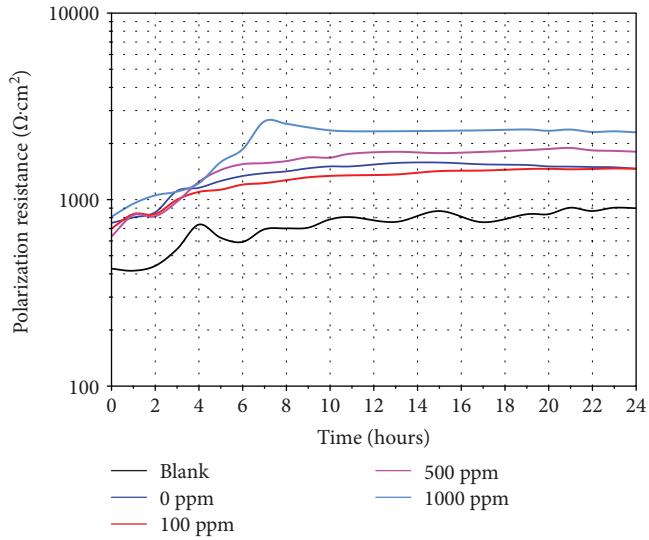

Figure 10: Variation in polarization resistance values for 1018 carbon steel bare and coated with chitosan doped with nanoparticles.

Figure S1 shows the morphological aspects of the $Nd_2Ti_2O_7$ nanoparticles synthesized. According to the micrographs, it is observed that the nanoparticles have an elongated shape close to an ellipsoidal shape with an average size of 100-200 nm.

3.2. Coating Deposition. Figure S2 shows the results of the effect of nanoparticle concentration on the thickness of the chitosan films deposited at 5 V as a function of time. It was observed that at deposition times greater than 20 minutes, the thickness of the chitosan films tends to decrease when increasing the nanoparticle concentration, and at a time of 20 minutes or less, the thicknesses obtained are similar. This indicates that the presence of nanoparticles, especially at high concentrations, acts as a barrier to the efficient deposition of chitosan. Furthermore, at large deposition times, the presence of surface defects due to the formation of trapped hydrogen bubbles increases. Therefore, a deposition voltage of 5 V and a deposition time of 20 minutes were established as an optimum condition for the deposition of chitosan films doped with nanoparticles. With these working conditions, it was possible to obtain chitosan films with similar thicknesses (≈4 microns) independently of the nanoparticle load (Figure S3).

3.3. Characterization of Chitosan Films. Figure 5 shows the FT-IR spectra of the chitosan films as a function of the concentration of nanoparticles. The FT-IR spectra of the chitosan films are a compilation of the different absorption bands that represent the different functional groups that comprise it. In all cases, it is observed that the spectra are characterized by the presence of wide broad bands, which indicates the superposition or combination of characteristic bands of functional groups.

FT-IR spectrum of the undoped chitosan film is characterized by [10, 14, 15, 32–38] a band at 670 cm^{-1} attributed to an out-of-plane flexion of the hydroxyl γ(OH.....O) involved in hydrogen bridges and a band around 1000 cm^{-1} due to the structure of the polysaccharide in addition to the glycosidic stretching bonds C-O and C-O-C (897-1150 cm^{-1}) that occur between the repetitive units of chitosan. The wide band located between 1300-2200 cm^{-1} is attributed to an overlap of signals such as the vibrations of amide I (1650-1665 cm^{-1}) and amide II (1550-1590 cm^{-1}), the flexions of CH2 (1425 cm^{-1}) and CH (1381 cm^{-1}), the bending vibrations of water molecules (1640 cm^{-1}), the C-N axial stretch (1420 cm^{-1}), and the N-H angular deformation (1380 cm^{-1}). The presence of water affects the previous stretch bands [36]. A second intense and wide band between 2800 and 3600 cm^{-1} is attributed to the axial stretching to both O-H, N-H (3450 cm^{-1}), and C-H (2850-2920 cm^{-1}) of the CH_2 and CH_3 groups, as well as to the stretching vibrations of physisorbed water molecules (3400 cm^{-1}).

The FT-IR spectrum of the chitosan films doped with 100 ppm of $Nd_2Ti_2O_7$ shows the same signals as those observed in the undoped chitosan film. The only difference is observed in the signals above 2800 cm^{-1}, that is to say, now the intense and wide band between 2800 and 3600 cm^{-1} is occupied by a well-defined signal in 2880 and 2910 cm^{-1} and a wide band between 3300 and 3500 cm^{-1} (3300, 3380, and 3455 cm^{-1}), where the signal observed at 2880 and 2910 cm^{-1} is associated with the stretching vibration of the pyranoid ring (νCH_2, νCH_3), and the signals observed at 3300, 3380, and 3455 cm^{-1} correspond to the axial stretching of the O-H bonds of the hydrogen bonds and N-H. The FT-IR spectrum of the chitosan films doped with 500 and 1000 ppm of $Nd_2Ti_2O_7$ shows the same signals as those observed in the chitosan film with 100 ppm of nanoparticles. The only appreciable difference is the wide and pronounced band observed between 650 and 1000 cm^{-1}, where this signal is associated with the structure of the polysaccharide (pyranoid ring). Due to the low concentration of nanoparticles, the FT-IR spectra do not show the characteristic bands of $Nd_2Ti_2O_7$ or they are overlapping with the characteristic bands of the chitosan.

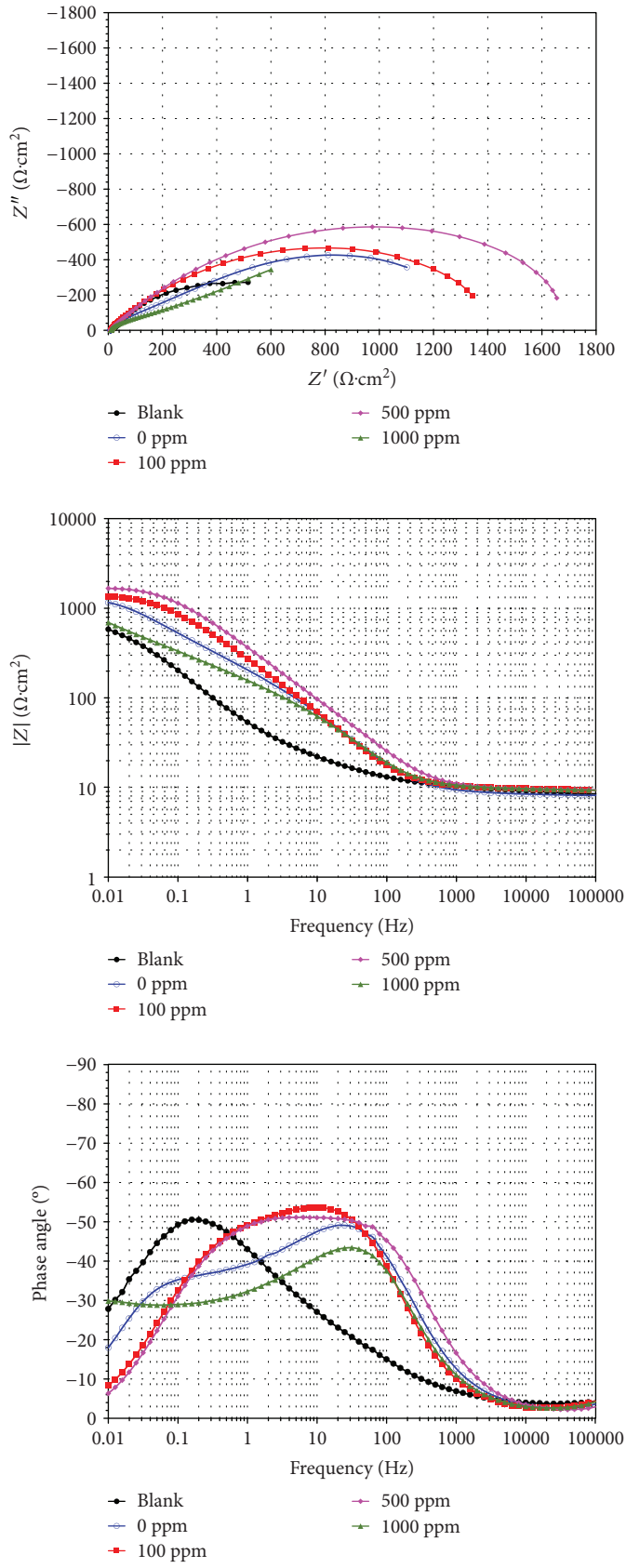

Figure 11: Nyquist and Bode diagrams for 1018 carbon steel bare and coated with chitosan doped with $Nd_2Ti_2O_7$ nanoparticles, after 24 hours of immersion in 3.5% NaCl solution.

From the analysis of the FT-IR spectra, it can be inferred that the chitosan films showed a high tendency to adsorb moisture, but with the addition of the nanoparticles, this decreases. This suggests an increase in the crystallinity of the chitosan films, because the amino group of chitosan forms a complex with the cationic part of the nanoparticles, as well as hydrogen bridges with its anionic part (hydroxyl or amino groups of chitosan) [39].

In Figure 6, the Raman spectra of the chitosan films are shown as a function of the concentration of nanoparticles added. The Raman spectrum of the chitosan film is characterized by [10, 15, 33, 40] a small broad band between 300 and 600 cm^{-1} attributed to the out-of-plane flexions of the OH groups and pyranoid ring (357-444 cm^{-1}), stretching of the C-O-C group (479 cm^{-1}), stretching of the CO-NH and C-CH_3 groups (493 cm^{-1}), and out-of-plane flexions of the NH, C=O, and CH_3 groups, in addition to the bending vibration in the plane of the pyranoid ring (566 cm^{-1}), and a prominent peak between 1100 and 2000 cm^{-1} attributed to the following signals: the axial stretching of the groups COC, CO, CC, C-OH, C-CH_2, CH, CH_2, and CH_3 and the pyranoid ring, in addition to the vibration of the flexion in the plane of the OH…O bond (1100-1300 cm^{-1}), as well as the flexion region of the CNH, amide III, amide II, and amide I groups (1375, 1445, 1540, and 1620 cm^{-1}, respectively. In all cases, a small shoulder is observed at 3264 cm^{-1} which corresponds to the stretching vibration (CH) of the pyranoid ring. In other Raman spectra reported in the literature, it has been observed that this signal is much more intense.

In the case of chitosan films doped with nanoparticles, it is observed that their Raman spectrum is practically identical to that of undoped chitosan. The only noticeable difference is the clearer definition of the signals already described. It has been reported that the Raman spectral bands of $Nd_2Ti_2O_7$ are located at 124, 172, 277, 347, 370, 440, 574, 614, 684, 794, and 824 cm^{-1} [22]. The absence of these characteristic bands in the Raman spectra of the doped chitosan films indicates the integration of the nanoparticles in the structure of the chitosan. This suggests an increase in the crystallinity of the chitosan films. The above discussion is in agreement with that discussed in the FT-IR spectra.

According to the FT-IR spectra, it had been concluded that the films showed a high tendency to adsorb moisture; however, due to the weak absorbance of the water in Raman spectroscopy [36], in this case, its presence is not evident. On the contrary, it was observed that the flexion bands of the CNH, amide III, amide II, and amide I groups were the most intensive bands of the Raman spectra. The presence of higher peaks with more defined reflections suggests a greater crystallinity or better packing of chitosan [41]. It has been indicated that an increase in the crystallinity of the polymer film reduces its permeability and its barrier properties are improved [42]. The evident presence of a large number of hydrogen bonds (FT-IR spectra) and prominent bands related to the amine groups (Raman spectra) suggests that the $Nd_2Ti_2O_7$ nanoparticles were complexed with the amine and hydroxyl groups of the polymer chain of chitosan.

Figure 7 shows the evolution of the DRX spectra of the chitosan films as a function of the nanoparticle concentration. It has been reported that the characteristic peaks of chitosan are located around 2θ values of 8°, 11°, 18°, and 23° [3, 15, 32, 33, 41, 43–47], where the first two peaks (8° and 11°) indicate a hydrated crystallite structure due to the integration of water molecules in the crystal lattice; the peak at 18° is attributed to the regular chitosan crystal lattice, and the peak around 23° corresponds to an amorphous chitosan structure [41]. Some studies report a diffraction peak around 15° which is attributed to an anhydrous crystalline network [33].

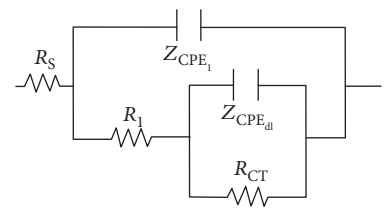

Figure 12: Equivalent circuit used to fit the impedance spectra.

According to the DRX spectrum of the undoped chitosan film, a wide peak can be observed around 8-11° and a second wide peak around 18-23°. The intensity of the first peak suggests a high degree of hydration and a poor crystallinity of the chitosan film, which is in agreement with what was discussed in the FT-IR and Raman spectra.

In the case of chitosan films doped with nanoparticles, the dominant diffraction pattern of the chitosan film is observed; however, by increasing the concentration of nanoparticles, the presence of diffraction peaks corresponding to $Nd_2Ti_2O_7$ is evident (Figure 3). Furthermore, it is observed that the intensity of the chitosan peak around 8-11° decreases, suggesting that the adsorption of moisture in the film decreases by increasing the nanoparticle content. Same observation was made in the discussion of the FT-IR and Raman spectra.

It should be noted that in all cases, the films deposited showed a yellow hue. It has been suggested that this is due to the presence of double bonds conjugated in its structure by the crosslinking of the film, which occurs when glutaraldehyde is used as a crosslinking agent [48].

3.4. Electrochemical Evaluation. Figure 8 shows the potentiodynamic polarization curves for 1018 carbon steel with and without chitosan coating (doped and undoped) evaluated in a 3.5% NaCl solution at room temperature. From the figure, it can be seen that carbon steel has a cathodic branch with a large slope; this allows inferring the existence of charge transfer limitations, and however, its anodic branch shows a low slope which indicates a high tendency to corrosion (metallic dissolution). Furthermore, the formation of a passive layer on its surface is not evident in the range of evaluated potentials.

However, in the case of carbon steel coated with undoped chitosan, its polarization curve showed a shift towards more active potentials and the slope of its cathodic branch decreased, and the slope of its anodic branch increased to potentials slightly above its corrosion potential (up to 100 mV). The observed changes allow inferring that the

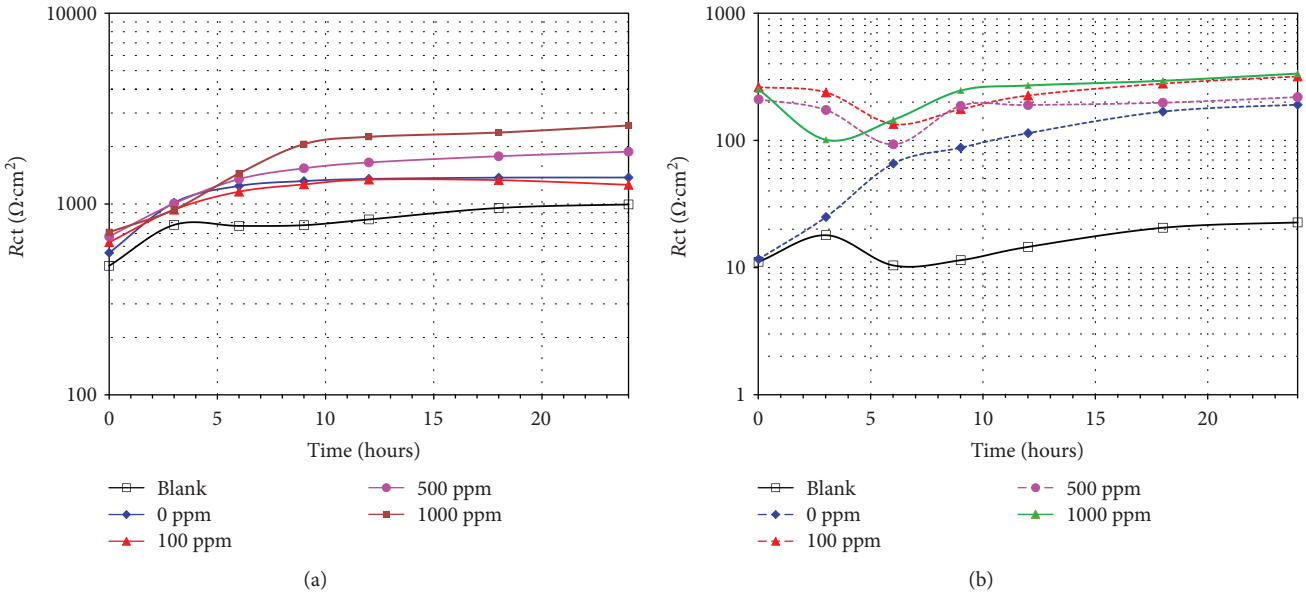

FIGURE 13: Evolution of the (a) R_{ct} and (b) R_1 values as a function of time for bare carbon steel and coated with a chitosan film with different concentrations of nanoparticles.

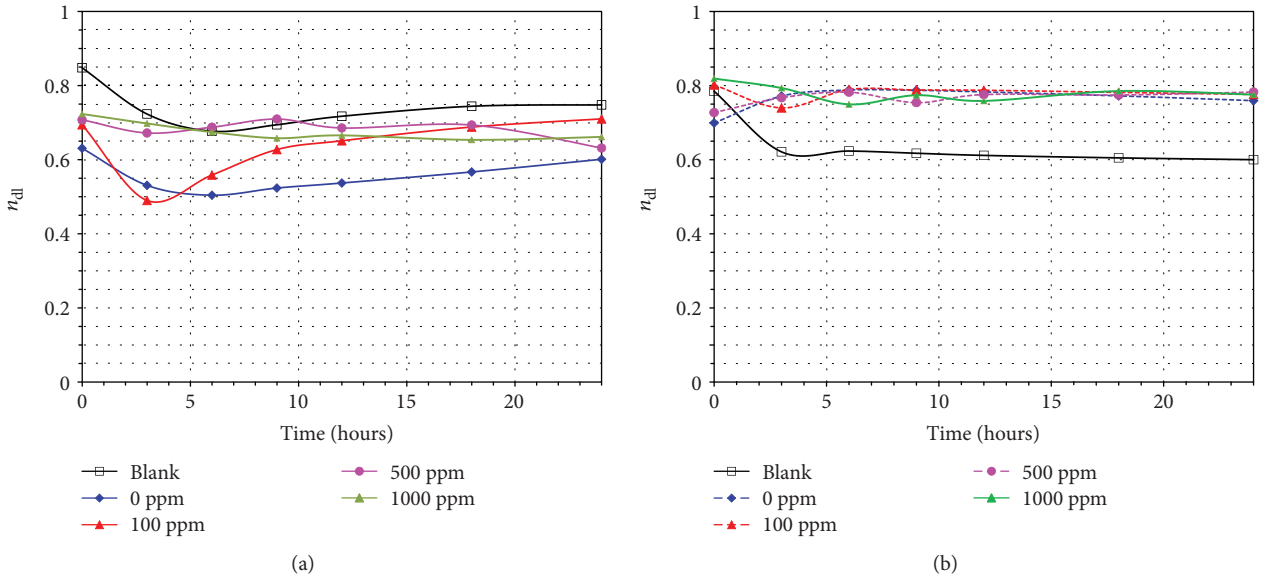

FIGURE 14: Evolution of the (a) n_{dl} and (b) n_1 values as a function of time for bare carbon steel and coated with a chitosan film with different concentrations of nanoparticles.

presence of the chitosan film decreases the dissolution rate of the carbon steel (increase in anodic slope), and due to the great displacement of the corrosion potential towards more active potentials (>200 mV), it acts as a cathodic coating affecting the oxygen reduction rate (cathodic reaction) and shifting the polarization curve to lower current densities [49].

The behavior of carbon steel coated with chitosan doped with nanoparticles is very similar to that observed in the presence of the undoped chitosan film. Although the variation in the I_{corr} values is not significant, the incorporation of nanoparticles seems to influence some variables of the corrosion process. The most significant changes are observed with the incorporation of 500 ppm of nanoparticles, namely, an increase in the slope of the anodic branch up to 160 mV above its corrosion potential, a more active corrosion potential, and a greater displacement of the cathodic branch at lower current densities. Polarization curves are an excellent tool to determine the protective capacity of the chitosan films deposited onto steel surface; however, the observed behavior simply corresponds to the beginning of the corrosion process. Therefore, in order to obtain a better response and

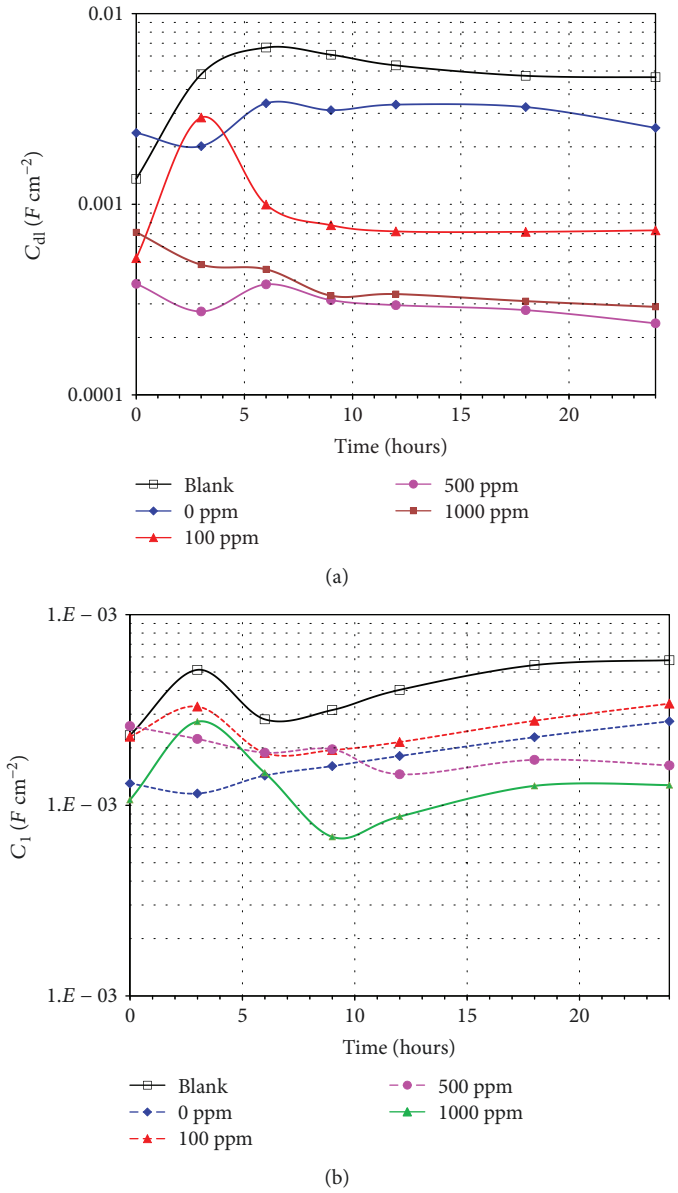

FIGURE 15: Evolution of the (a) C_{dl} and (b) C_1 values as a function of time for bare carbon steel and coated with a chitosan film with different concentrations of nanoparticles.

behavior of deposited films, it is necessary to carry out performance tests at longer times by means of complementary electrochemical techniques such as OCP, RPL, and EIS measurements. Table 1 shows the electrochemical parameters obtained from the polarization curves.

Figure 9 shows the variation of the OCP as a function of time for 1018 carbon steel with and without chitosan coating (doped and undoped) evaluated in 3.5% NaCl solution at room temperature. In the case of bare carbon steel, it was observed that it showed a drop in its OCP values (≈30 mV) in the first hour of immersion and then a constant decrease until the end of the test without reaching the steady state. It is known that an increase in the OCP values indicates the formation of a passive film on the material surface, and on the contrary, a decrease in its values shows a continuous corrosion process, as well as the presence of constant values indicates a surface stable [50]. Based on the above discussion, it can be assumed that bare carbon steel undergoes a continuous corrosion process and is not capable of developing a stable corrosion product layer that decreases its corrosion rate.

However, in the presence of a chitosan film (with or without nanoparticles) in all cases, an abrupt drop in the OCP values is observed in the first hours of immersion and subsequently their values remain practically stable. The drop in OCP values is averaged from 90 to 110 mV. Some authors suggest that an abrupt initial drop in the OCP values is associated with processes of reorganization of the surface layers as a result of an increase in the metallic dissolution or a decrease in the cathodic reactions [51, 52]. However, in this case, it can be assumed that the observed drop in OCP values may be due to the sorption and absorption of water in the chitosan film, which causes its swelling [41, 48, 53].

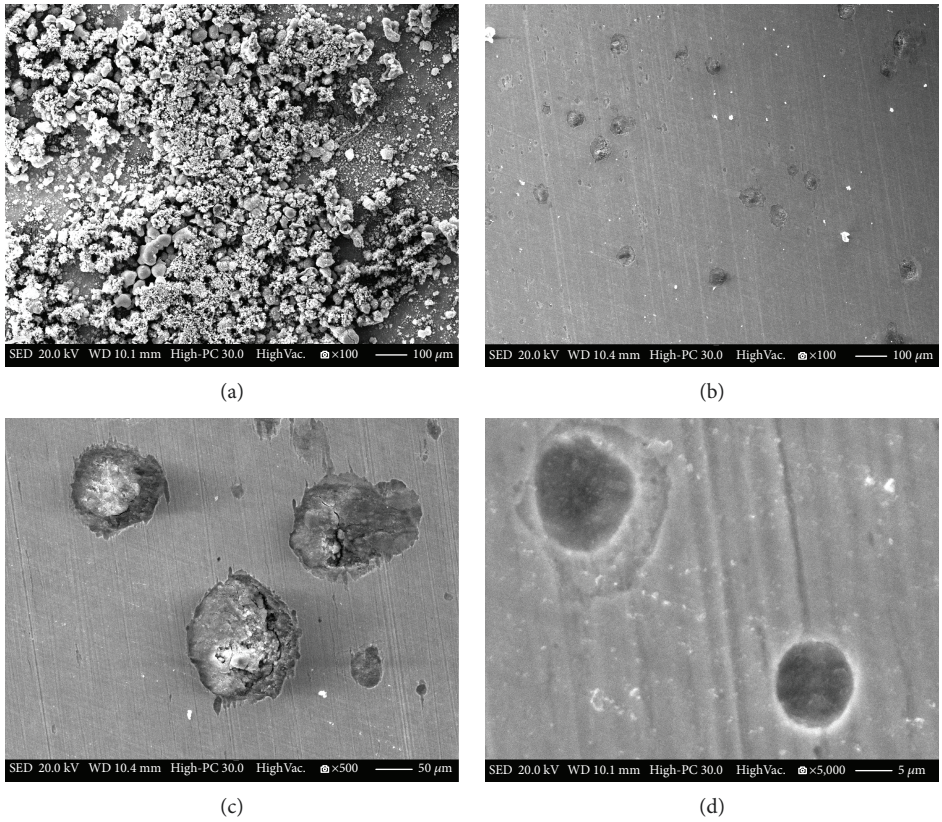

Figure 16: Morphological aspects of carbon steel after 24 hours of immersion in a 3.5% NaCl solution at room temperature.

After this, it is observed that the OCP values remain practically stationary; this shows the protective nature of the films deposited.

In the case of corrosion inhibitors, it has been suggested that when they cause a displacement in OCP values greater than ±85 mV, with respect to the blank, they can be defined as anodic or cathodic inhibitors depending on the direction of displacement [49, 54–56]. Therefore, in this case, it can be assumed that the deposited chitosan films act as cathodic coating based on the displacement caused in the OCP values with respect to bare carbon steel.

Figure 10 shows the variation in LPR as a function of time for 1018 carbon steel with and without chitosan coating (doped and undoped) evaluated in 3.5% NaCl solution at room temperature. The evolution of the polarization resistance values of the bare carbon steel shows a tendency to increase constantly without reaching the steady state in the evaluated test period. This behavior can be due to the continuous corrosion process which causes the accumulation of corrosion products on the surface, limiting the diffusion of the electrolyte but without forming a compact barrier. The above discussion is in accordance with the trend observed in the evolution of its OCP values. In the case of carbon steel coated with chitosan films, in all cases, higher initial resistance values were observed with respect to bare carbon steel. This indicates that the chitosan films increase the corrosion resistance of carbon steel. At higher immersion times, a constant increase in the resistance values is observed until reaching a quasistationary state depending on the nanoparticle concentration. In the case of chitosan films with 0 and 100 ppm, a similar behavior is observed; however, at higher concentrations, the resistance values tend to increase with the nanoparticle concentration. This increase in the resistance values may be due to a barrier effect that reduces the effective area for the migration of the aggressive species towards the metallic surface.

Figure 11 shows the Nyquist and Bode diagrams for 1018 carbon steel with and without chitosan coating (doped and undoped) evaluated in 3.5% NaCl solution at room temperature after 24 hours of testing. According to the Nyquist diagram, carbon steel shows the apparent presence of a single depressed capacitive semicircle with a diameter of less than 800 Ohm·cm^2. However, the analysis of the Bode diagram in its phase angle format shows the presence of an apparent time constant around 0.2 Hz with a maximum phase angle of 50°, but its shape does not show symmetry (like a Gauss bell); therefore, it is possible that in reality, there are two overlapping time constants whose response surface is the observed one. According to this, it is possible to infer that the first time constant is in the intermediate frequency region between 10 and 100 Hz. The above is corroborated when analyzing the Bode diagram in its impedance module format, $|Z|$, in which it is possible to observe three slopes in the relation log f vs. log |Z|. The first slope is located in the high-frequency region (>1000 Hz), which corresponds to the solution resistance; the second slope is located in

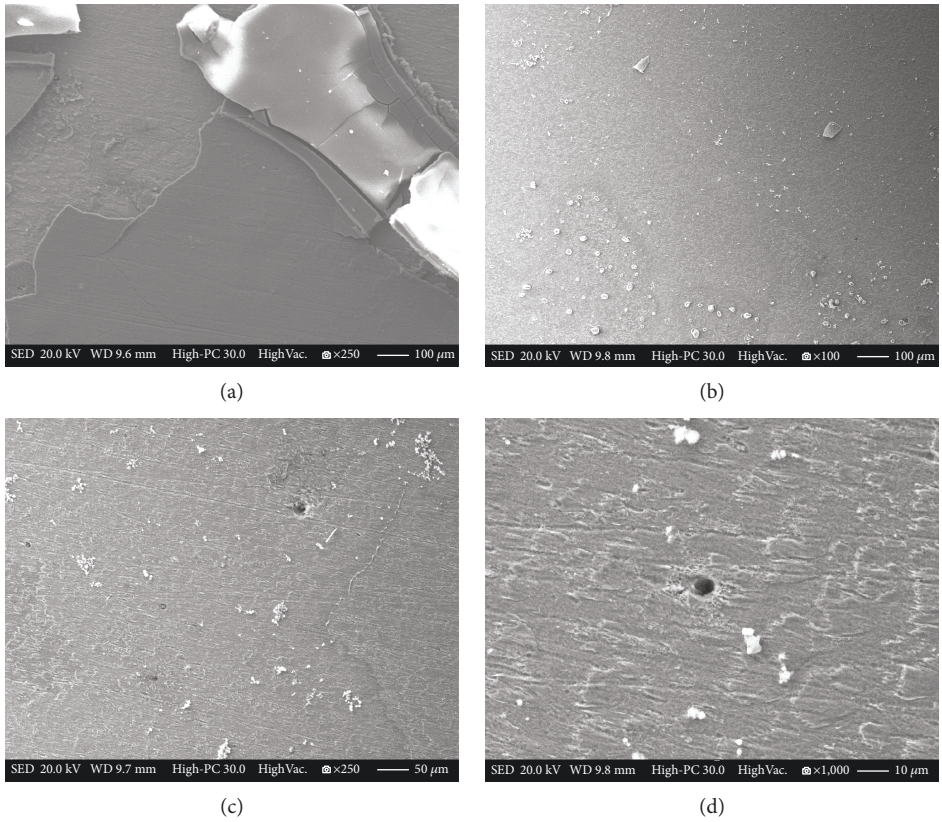

Figure 17: Morphological aspects of carbon steel coated with a chitosan film after 24 hours of immersion in a 3.5% NaCl solution at room temperature.

the intermediate-frequency region (10-100 Hz), which corresponds to the first time constant which can be associated with the presence of a corrosion product layer; and the third slope is located in the region of low frequency (maximum phase angle), which corresponds to the second time constant associated with the capacitive response of the metallic surface. In addition, it is not possible to define the low-frequency plateau which indicates that the charge transfer resistance (R_{ct}) is greater than the last registered value. It is common that in the Nyquist diagram, the real time constants associated with the corrosion process are not observed; this is due to the fact that the first time constants generally evolve between the high-frequency region and the intermediate-frequency region, and in the Nyquist diagram, the most visible experimental data correspond to the low-frequency region [49, 51].

On the other hand, carbon steel coated with a film of chitosan (doped and undoped) from its Nyquist diagram also shows the apparent presence of a single capacitive semicircle whose diameter is greater than that observed for bare carbon steel. This indicates that the presence of the chitosan film increased the charge transfer resistance of the steel. The analysis of the Bode diagrams shows the well-defined presence of two time constants. According to the Bode diagram in its phase angle format, it is observed that the maximum phase angles of the time constants are located around 100 Hz and 0.1 Hz. From the Bode diagram in its impedance module format, |Z|, the slope changes associated to the time constants are observed. In all cases, the development of the low-frequency plateau is not evident. The evolution as a function of time of the impedance spectra is shown in Supplementary Materials.

The impedance spectra were adapted by means of the equivalent circuit shown in Figure 12.

In this case, R_s represents the solution resistance, R_1 and CPE_1 are the resistance and the constant phase element either of the corrosion product layer or of the chitosan film in the case of bare or coated steel, respectively, and R_{ct} and CPE_{dl} are the charge transfer resistance and the capacitance of the electrochemical double layer, respectively.

The capacitances have been replaced by CPE to compensate the surface irregularities, where the CPE impedance is defined as follows:

$$Z_{CPE} = \left(\frac{1}{Y_0}\right)(j\omega)^{-n}. \quad (1)$$

In this case, Y_0 is the constant or magnitude of the CPE ($F\,cm^{-2}\,s^{(n-1)}$), ω is the angular frequency ($rad\,s^{-1}$), $j^2 = -1$ is the imaginary number, and n is a phenomenological coefficient that indicates the phase shift and represents the heterogeneity of the surface; their values can be $0 < n < 1$. If $n = 1$, $CPE = C = 1/Y_0$; if $n = 0.5$, $CPE = Z_W$ (Warburg

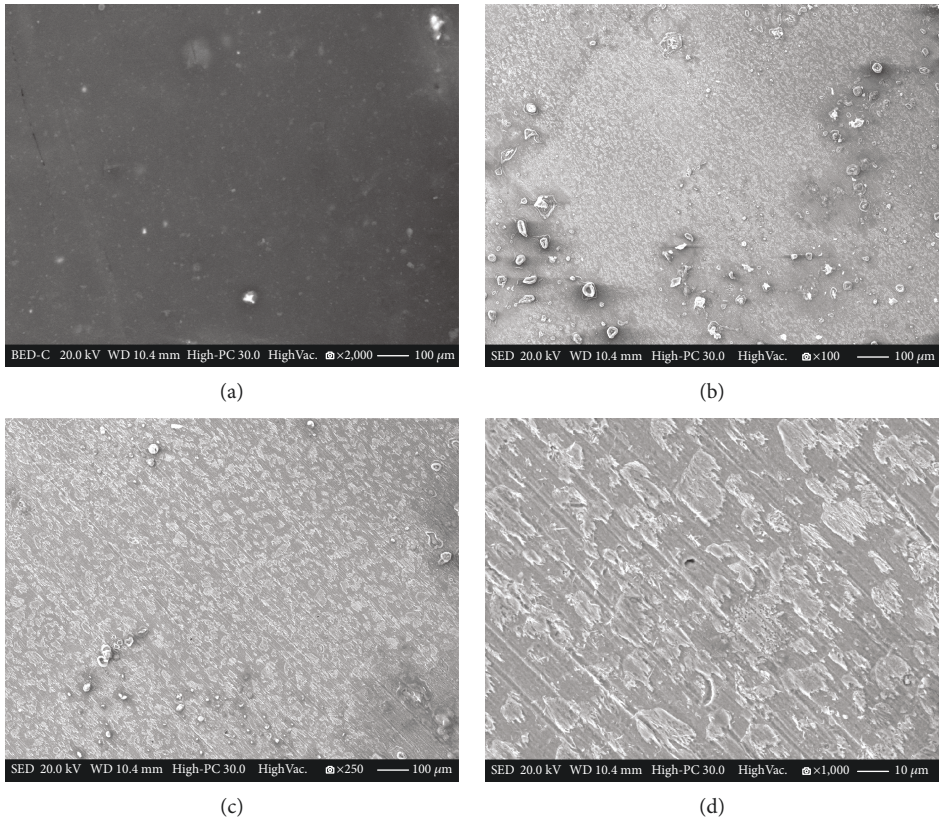

Figure 18: Morphological aspects of carbon steel coated with a film of chitosan doped with 100 ppm of nanoparticles, after 24 hours of immersion in a 3.5% NaCl solution at room temperature.

impedance); if $n = 0$, CPE = R. The capacitance of the CPE can be calculated using the following equation [57]:

$$C_{\mathrm{CPE}} = \frac{(Y_0 R)^{1/n}}{R}. \quad (2)$$

Figures 13–15 show the evolution of the electrochemical parameters obtained from the fitting of the impedance spectra. Figure 13 shows the evolution of the values of R_{ct} and R_1 of bare carbon steel and coated with a chitosan film with different concentrations of nanoparticles. It is observed that the R_{ct} values and its tendency are similar to those observed in the polarization resistance measurements (R_{p}); this indicates that the equivalent circuit used represents the surface processes detected by means of the electrochemical impedance measurements. The possible differences may be due to the fact that in general $R_{\mathrm{p}} \approx R_{\mathrm{ct}} + R_1$. On the other hand, the R_1 values show that the resistance of the chitosan film increases with the nanoparticles content, and that once the steady state is reached $(t > 6\,\mathrm{h})$, their resistance values are similar to the initial ones. It is possible that the increase in the chitosan film resistance (without nanoparticles) is due to the increase in its thickness due to the electrolyte absorption. The above discussion suggests that the moisture absorption capacity of chitosan films doped with nanoparticles is decreased.

Figure 14 shows the evolution of the n_{dl} and n_1 values for bare carbon steel and coated with a chitosan film with different concentrations of nanoparticles. Regarding the values of n_{dl}, it is observed that the chitosan film has the lowest values and close to 0.5; however, these values increase with the nanoparticle content but they are slightly lower than those of bare steel. On the other hand, with respect to the values of n_1, it is observed that all chitosan films show similar and larger values to those of bare steel. This suggests that the presence of the chitosan film improved the surface uniformity regardless of its nanoparticle content.

Figure 15 shows the evolution of the values of C_{dl} and C_1 for bare carbon steel and coated with a film of chitosan with different concentrations of nanoparticles. The bare carbon steel initially showed a rapid increase in its C_{dl} values and, in general, the highest values. This indicates a greater susceptibility to corrosion. On the other hand, the chitosan film without nanoparticles also showed an initial increase in its C_{dl} values but its values were always lower than those of bare steel. However, in the presence of nanoparticles, all the films showed lower values of C_{dl} and these decreased by increasing the concentration of nanoparticles. This indicates that the presence of nanoparticles increased the corrosion resistance of carbon steel. Regarding the values of C_1, it is observed that bare carbon steel showed the highest values which indicate the low protective properties of its corrosion product layer. However, in the presence of a chitosan film on its surface, lower C_1 values are observed but with a tendency to increase, possibly due to the absorption of electrolyte. With the addition of 100 ppm of nanoparticles, a behavior similar

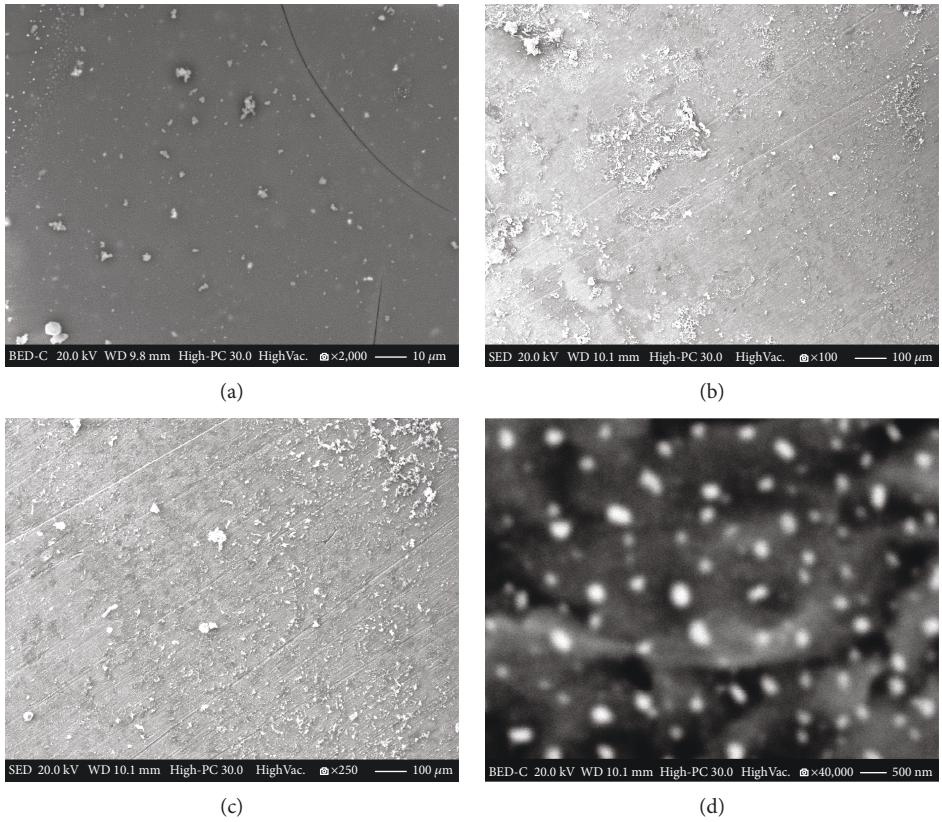

Figure 19: Morphological aspects of carbon steel coated with a film of chitosan doped with 500 ppm of nanoparticles, after 24 hours of immersion in a 3.5% NaCl solution at room temperature.

to that shown with 0 ppm is observed; this may be due to the low amount of nanoparticles. However, by increasing the concentration of nanoparticles, it is observed that the C_1 values are the lowest once the steady state has been reached. This suggests a more protective character of the chitosan films. The results shown suggest that a higher concentration of nanoparticles than those reported here may result in the formation of chitosan films with greater anticorrosive properties.

3.5. Morphological Analysis of Corroded Surfaces. Figure 16 shows the morphological aspects of the 1018 carbon steel surface after the corrosion process for 24 hours in a 3.5% NaCl solution at room temperature. The presence of a large amount of corrosion products of a nonprotective nature was observed on the surface of the steel (Figure 16(a)). This was evident by eliminating the corrosion products and observing the presence of strong pitting damage on its surface (Figures 16(b)–16(d)). The presence of large pits (>50 microns) and a high density of smaller pits (<5 microns) was observed. The micrographs clearly show that the carbon steel underwent a nonuniform corrosion process with a strong pitting attack.

Figure 17 shows the morphological aspects of the 1018 carbon steel surface coated with chitosan after the corrosion process for 24 hours in a 3.5% NaCl solution at room temperature. From Figure 17(a), it can be seen that the chitosan film remained free of corrosion products on its surface (the observed cracking was due to the drying process and to the high vacuum conditions used for its observation). Figures 17(b)–17(d) show the surface aspects of the steel after the chitosan film has been removed. It is evident that the attack experienced by the carbon steel was lower; although the presence of pitting is appreciated, its magnitude and density was low. The observed attack could be due to the presence of superficial defects in the chitosan film.

Figures 18–20 show the morphological aspects of the surface of 1018 carbon steel coated with doped chitosan with different concentrations of nanoparticles, after the corrosion process for 24 hours in a 3.5% NaCl solution at room temperature. Figures 18(a), 19(a), and 20(a) show the surface appearance of the chitosan film as a function of the concentration of added nanoparticles, 100 ppm, 500 ppm, and 1000 ppm, respectively. In general, the surface shows a less homogeneous appearance than that observed in the absence of nanoparticles; this may be due to the formation of nanoparticle clusters in the outer layers of the chitosan film. The detachment of the chitosan films was more difficult. On the surface of the steel, the presence of very thin chitosan layers strongly adhered was observed. It is noticeable that the surface attack was less; smaller pits were observed than those observed in the presence of the undoped chitosan film. In particular in Figures 19(d) and 20(d), the images of backscattered electrons are shown where it is possible to observe a thin chitosan layer adhered to the steel surface and the presence of the codeposited nanoparticles.

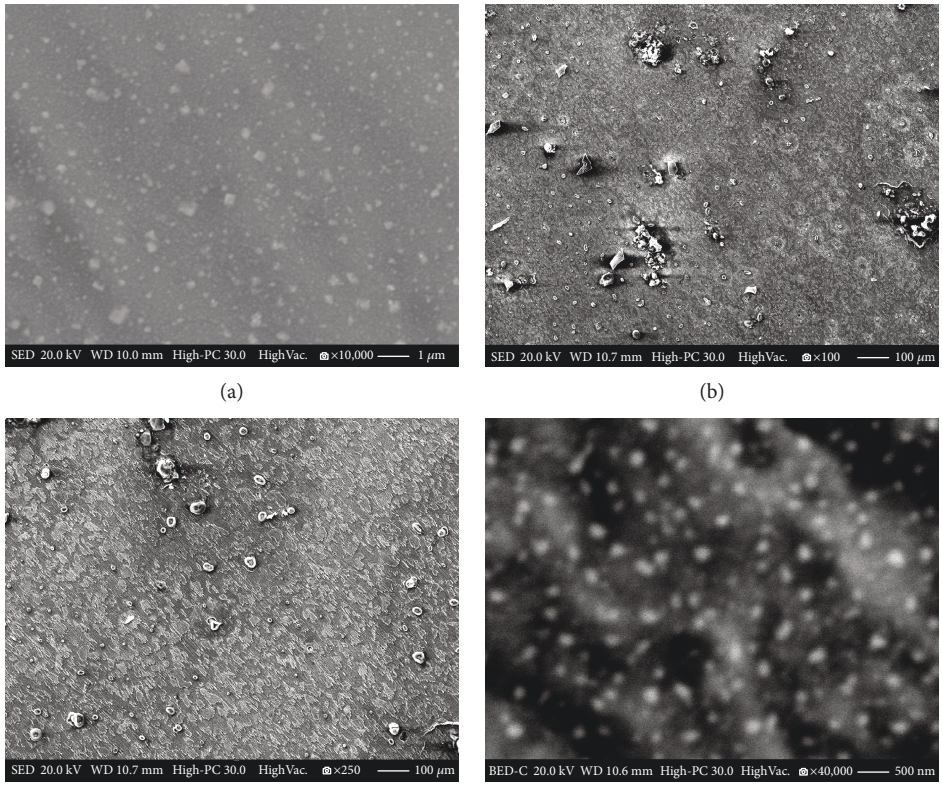

Figure 20: Morphological aspects of carbon steel coated with a film of chitosan doped with 1000 ppm of nanoparticles, after 24 hours of immersion in a 3.5% NaCl solution at room temperature.

The above evidences show that chitosan films doped with nanoparticles improved the anticorrosive properties of carbon steel. It is possible that the increase in corrosion resistance of steel is due to the fact that nanoparticles acted as a solid barrier for the free diffusion of reactants by reducing the effective area of diffusion.

4. Conclusions

The results obtained show that the synthesis process of $Nd_2Ti_2O_7$ allows obtaining nanoparticles completely crystalline with an average size of 100-200 nm. It was possible to deposit homogeneous chitosan films with 4 microns thickness independently of the concentration of nanoparticles applying a 5 V potential for 20 minutes. The characterization of the chitosan films shows that the nanoparticle codeposition reduces their moisture adsorption capacity and increases the crystallinity of the deposited films. Electrochemical evaluation of the chitosan films shows a clear decrease in the corrosion current density and an increase in the polarization resistance and in the charge transfer resistance by increasing the concentration of codeposited nanoparticles. Likewise, a decrease in the values of corrosion potential and open circuit potential was observed. These characteristics indicate that the films deposited reduce the anodic reaction (reduction of oxygen) and due to this the corrosion rate of the protected material.

Data Availability

The data used to support the findings of this study are available from the corresponding author upon request.

Conflicts of Interest

The authors declare that there are no conflicts of interest regarding the publication of this paper.

Acknowledgments

Financial support from the Consejo Nacional de Ciencia y Tecnología (CONACYT, México) (Project 232611 "Laboratorio Nacional de Materias Primas, Metalurgia y Aleaciones Estratégicas Basadas en Tierras Raras Orientadas a Fortalecer la Sustentabilidad de los Sectores Energía, Transporte y Comunicaciones") is gratefully acknowledged. The authors are grateful for the comments and support provided by M. Casales-Diaz and J.J. Ramos-Hernandez.

Supplementary Materials

Morphological aspects of the $Nd_2Ti_2O_7$ nanoparticles. Figure S1: morphological aspect of the $Nd_2Ti_2O_7$ nanoparticles synthesized. Figure S2: effect of the nanoparticle concentration on the thickness of the chitosan films (deposition voltage = 5 V). Figure S3: appearance in cross section of the chitosan films according to the concentration of nanoparticles. Figure

S4: Nyquist and Bode diagrams for 1018 carbon steel evaluated in 3.5% NaCl solution. Figure S5: Nyquist and Bode diagrams for 1018 carbon steel coated with chitosan evaluated in 3.5% NaCl solution. Figure S6: Nyquist and Bode diagrams for 1018 carbon steel coated with chitosan doped with 100 ppm of nanoparticles in 3.5% NaCl solution. Figure S7: Nyquist and Bode diagrams for 1018 carbon steel coated with chitosan doped with 500 ppm of nanoparticles in 3.5% NaCl solution. Figure S8: Nyquist and Bode diagrams for 1018 carbon steel coated with chitosan doped with 1000 ppm of nanoparticles in 3.5% NaCl solution. *(Supplementary Materials)*

References

[1] H. Hassannejad and A. Nouri, "Synthesis and evaluation of self-healing cerium-doped chitosan nanocomposite coatings on AA5083-H321," *International Journal of Electrochemical Science*, vol. 11, pp. 2106–2118, 2016.

[2] J. Carneiro, J. Tedim, S. C. M. Fernandes et al., "Chitosan as a smart coating for controlled release of corrosion inhibitor 2-mercaptobenzothiazole," *ECS Electrochemistry Letters*, vol. 2, no. 6, pp. C19–C22, 2013.

[3] S. John, A. Joseph, A. J. Jose, and B. Narayana, "Enhancement of corrosion protection of mild steel by chitosan/ZnO nanoparticle composite membranes," *Progress in Organic Coatings*, vol. 84, pp. 28–34, 2015.

[4] J. Carneiro, J. Tedim, S. C. M. Fernandes et al., "Functionalized chitosan-based coatings for active corrosion protection," *Surface and Coatings Technology*, vol. 226, pp. 51–59, 2013.

[5] J. Carneiro, J. Tedim, S. C. M. Fernandes et al., "Chitosan--based self-healing protective coatings doped with cerium nitrate for corrosion protection of aluminum alloy 2024," *Progress in Organic Coatings*, vol. 75, no. 1-2, pp. 8–13, 2012.

[6] R. A. Farghali, A. M. Fekry, R. A. Ahmed, and H. K. A. Elhakim, "Corrosion resistance of Ti modified by chitosan–gold nanoparticles for orthopedic implantation," *International Journal of Biological Macromolecules*, vol. 79, pp. 787–799, 2015.

[7] A. S. Bhatt, D. K. Bhat, and M. S. Santosh, "Electrochemical properties of chitosan–Co_3O_4 nanocomposite films," *Journal of Electroanalytical Chemistry*, vol. 657, no. 1-2, pp. 135–143, 2011.

[8] A. S. Bhatt, D. Krishna Bhat, and M. S. Santosh, "Electrical and magnetic properties of chitosan-magnetite nanocomposites," *Physica B: Condensed Matter*, vol. 405, no. 8, pp. 2078–2082, 2010.

[9] J. Jung, G. M. Raghavendra, D. Kim, and J. Seo, "Improving properties of Hanji by coating chitosan–silver nanoparticle solution," *International Journal of Biological Macromolecules*, vol. 93, pp. 933–939, 2016.

[10] M. L. Zheludkevich, J. Tedim, C. S. R. Freire et al., "Self-healing protective coatings with "green" chitosan based pre-layer reservoir of corrosion inhibitor," *Journal of Materials Chemistry*, vol. 21, no. 13, pp. 4805–4812, 2011.

[11] T. Wu, Y. Li, and D. S. Lee, "Chitosan-based composite hydrogels for biomedical applications," *Macromolecular Research*, vol. 25, no. 6, pp. 480–488, 2017.

[12] G. Kumar and R. G. Buchheit, "Development and characterization of corrosion resistant coatings using the natural biopolymer chitosan," *ECS Transactions*, vol. 1, no. 9, pp. 101–117, 2006.

[13] S. A. Umoren, M. J. Banera, T. Alonso-Garcia, C. A. Gervasi, and M. V. Mirifico, "Inhibition of mild steel corrosion in HCl solution using chitosan," *Cellulose*, vol. 20, no. 5, pp. 2529–2545, 2013.

[14] L.-Q. Wu, A. P. Gadre, H. Yi et al., "Voltage-dependent assembly of the polysaccharide chitosan onto an electrode surface," *Langmuir*, vol. 18, no. 22, pp. 8620–8625, 2002.

[15] R. Nirmala, B. W. Il, R. Navamathavan, M. H. El-Newehy, and H. Y. Kim, "Preparation and characterizations of anisotropic chitosan nanofibers via electrospinning," *Macromolecular Research*, vol. 19, no. 4, pp. 345–350, 2011.

[16] S. Kaur and G. S. Dhillon, "The versatile biopolymer chitosan: potential sources, evaluation of extraction methods and applications," *Critical Reviews in Microbiology*, vol. 40, no. 2, pp. 155–175, 2014.

[17] I. Zhitomirsky and A. Hashambhoy, "Chitosan-mediated electrosynthesis of organic–inorganic nanocomposites," *Journal of Materials Processing Technology*, vol. 191, no. 1-3, pp. 68–72, 2007.

[18] R. A. Ahmed, R. A. Farghali, and A. M. Fekry, "Study for the stability and corrosion inhibition of electrophoretic deposited chitosan on mild steel alloy in acidic medium," *International Journal of Electrochemical Science*, vol. 7, pp. 7270–7282, 2012.

[19] I. Zhitomirsky, "Electrophoretic deposition of organic–inorganic nanocomposites," *Journal of Materials Science*, vol. 41, no. 24, pp. 8186–8195, 2006.

[20] S. Heydarian, Z. Ranjbar, and S. Rastegar, "Electrophoretic deposition behavior of chitosan biopolymer as a function of solvent type," *Polymer-Plastics Technology and Engineering*, vol. 54, no. 11, pp. 1193–1200, 2015.

[21] M. M. Milanova, M. Kakihana, M. Arima, M. Yashima, and M. Yoshimura, "A simple solution route to the synthesis of pure $La_2Ti_2O_7$ and $Nd_2Ti_2O_7$ at 700–800°C by polymerized complex method," *Journal of Alloys and Compounds*, vol. 242, no. 1-2, pp. 6–10, 1996.

[22] K. Krishnankutty and K. R. Dayas, "Synthesis and characterization of monoclinic rare earth titanates, $RE_2Ti_2O_7$ (RE = La, Pr, Nd), by a modified SHS method using inorganic activator," *Bulletin of Materials Science*, vol. 31, no. 6, pp. 907–918, 2008.

[23] D. S. Todorovsky, M. M. Getsova, M. M. Milanova et al., "The chemistry of the processes involved in the production of lanthanide titanates by the polymerized-complex method," *Canadian Journal of Chemistry*, vol. 85, no. 7-8, pp. 547–559, 2007.

[24] M. Suresh, A. V. Prasadarao, and S. Komarneni, "Mixed hydroxide precursors for La2Ti2O7 and Nd2Ti2O7 by homogeneous precipitation," *Journal of Electroceramics*, vol. 6, no. 2, pp. 147–151, 2001.

[25] S. Cizauskaite, V. Reichlova, G. Nenartaviciene, A. Beganskiene, J. Pinkas, and A. Kareiva, "Sol–gel preparation and characterization of gadolinium aluminate," *Materials Chemistry and Physics*, vol. 102, no. 1, pp. 105–110, 2007.

[26] M. Motta, C. V. Deimling, M. J. Saeki, and P. N. Lisboa-Filho, "Chelating agent effects in the synthesis of mesoscopic-size superconducting particles," *Journal of Sol-Gel Science and Technology*, vol. 46, no. 2, pp. 201–207, 2008.

[27] V. V. Atuchin, T. A. Gavrilova, J. C. Grivel, and V. G. Kesler, "Electronic structure of layered titanate $Nd_2Ti_2O_7$," *Surface Science*, vol. 602, no. 19, pp. 3095–3099, 2008.

[28] Z. Shao, S. Saitzek, P. Roussel et al., "An easy sol–gel route for deposition of oriented $Ln_2Ti_2O_7$ (Ln=La, Nd) films on $SrTiO_3$

substrates," *Journal of Crystal Growth*, vol. 311, no. 16, pp. 4134–4141, 2009.

[29] W. Gong and R. Zhang, "Phase relationship in the TiO_2–Nd_2O_3 pseudo-binary system," *Journal of Alloys and Compounds*, vol. 548, pp. 216–221, 2013.

[30] T. Pussacq, H. Kabbour, S. Colis et al., "Reduction of $Ln_2Ti_2O_7$ layered perovskites: a survey of the anionic lattice, electronic features, and potentials," *Chemistry of Materials*, vol. 29, no. 3, pp. 1047–1057, 2017.

[31] Z. Zhao, Y. Zhang, J. Yang, H. Li, W. Song, and X. Zhao, "Low-temperature synthesis of $La_2Ti_2O_7$ nanocrystal by metallorganic decomposition method," *Journal of the Ceramic Society of Japan*, vol. 113, no. 1313, pp. 67–70, 2005.

[32] O. A. C. Monteiro Jr. and C. Airoldi, "Some studies of crosslinking chitosan–glutaraldehyde interaction in a homogeneous system," *International Journal of Biological Macromolecules*, vol. 26, no. 2-3, pp. 119–128, 1999.

[33] K. V. Harish Prashanth, F. S. Kittur, and R. N. Tharanathan, "Solid state structure of chitosan prepared under different N-deacetylating conditions," *Carbohydrate Polymers*, vol. 50, no. 1, pp. 27–33, 2002.

[34] A. Zając, J. Hanuza, M. Wandas, and L. Dymińska, "Determination of N-acetylation degree in chitosan using Raman spectroscopy," *Spectrochimica Acta Part A: Molecular and Biomolecular Spectroscopy*, vol. 134, pp. 114–120, 2015.

[35] I. K. D. Dimzon and T. P. Knepper, "Degree of deacetylation of chitosan by infrared spectroscopy and partial least squares," *International Journal of Biological Macromolecules*, vol. 72, pp. 939–945, 2015.

[36] S. Beil, A. Schamberger, W. Naumann, S. Machill, and K.-H. van Pée, "Determination of the degree of N-acetylation (DA) of chitin and chitosan in the presence of water by first derivative ATR FTIR spectroscopy," *Carbohydrate Polymers*, vol. 87, no. 1, pp. 117–122, 2012.

[37] F. Gebhardt, S. Seuss, M. C. Turhan, H. Hornberger, S. Virtanen, and A. R. Boccaccini, "Characterization of electrophoretic chitosan coatings on stainless steel," *Materials Letters*, vol. 66, no. 1, pp. 302–304, 2012.

[38] M. Mehdipour and A. Afshar, "A study of the electrophoretic deposition of bioactive glass–chitosan composite coating," *Ceramics International*, vol. 38, no. 1, pp. 471–476, 2012.

[39] R. Hirase, Y. Higashiyama, M. Mori, Y. Takahara, and C. Yamane, "Hydrated salts as both solvent and plasticizer for chitosan," *Carbohydrate Polymers*, vol. 80, no. 3, pp. 993–996, 2010.

[40] D. S. dos Santos, P. J. G. Goulet, N. P. W. Pieczonka, O. N. Oliveira, and R. F. Aroca, "Gold nanoparticle embedded, self-sustained chitosan films as substrates for surface-enhanced Raman scattering," *Langmuir*, vol. 20, no. 23, pp. 10273–10277, 2004.

[41] A. Giannakas, K. Grigoriadi, A. Leontiou, N.-M. Barkoula, and A. Ladavos, "Preparation, characterization, mechanical and barrier properties investigation of chitosan–clay nanocomposites," *Carbohydrate Polymers*, vol. 108, pp. 103–111, 2014.

[42] N. S. Sangaj and V. C. Malshe, "Permeability of polymers in protective organic coatings," *Progress in Organic Coatings*, vol. 50, no. 1, pp. 28–39, 2004.

[43] S. M. Rafigh and A. Heydarinasab, "Mesoporous chitosan–SiO_2 nanoparticles: synthesis, characterization, and CO_2 adsorption capacity," *ACS Sustainable Chemistry & Engineering*, vol. 5, no. 11, pp. 10379–10386, 2017.

[44] H. H. H. Hefni, E. M. Azzam, E. A. Badr, M. Hussein, and S. M. Tawfik, "Synthesis, characterization and anticorrosion potentials of chitosan-*g*-PEG assembled on silver nanoparticles," *International Journal of Biological Macromolecules*, vol. 83, pp. 297–305, 2016.

[45] X. Pang and I. Zhitomirsky, "Electrodeposition of composite hydroxyapatite–chitosan films," *Materials Chemistry and Physics*, vol. 94, no. 2-3, pp. 245–251, 2005.

[46] C. Liu and R. Bai, "Preparation of chitosan/cellulose acetate blend hollow fibers for adsorptive performance," *Journal of Membrane Science*, vol. 267, no. 1-2, pp. 68–77, 2005.

[47] J. Zhao, W. Han, H. Chen et al., "Preparation, structure and crystallinity of chitosan nano-fibers by a solid–liquid phase separation technique," *Carbohydrate Polymers*, vol. 83, no. 4, pp. 1541–1546, 2011.

[48] C. Tual, E. Espuche, M. Escoubes, and A. Domard, "Transport properties of chitosan membranes: influence of crosslinking," *Journal of Polymer Science Part B: Polymer Physics*, vol. 38, no. 11, pp. 1521–1529, 2000.

[49] D. M. Martinez de la Escalera, J. J. Ramos-Hernandez, E. Porcayo-Palafox, J. Porcayo-Calderon, J. G. Gonzalez-Rodriguez, and L. Martinez-Gomez, "Effect of Nd^{3+} ion concentration on the corrosion resistance of API X70 steel in chloride-rich environments," *Advances in Materials Science and Engineering*, vol. 2018, Article ID 9328317, 15 pages, 2018.

[50] I. Gurappa, "Characterization of different materials for corrosion resistance under simulated body fluid conditions," *Materials Characterization*, vol. 49, no. 1, pp. 73–79, 2002.

[51] Y. Zhu, J. Zhuang, Y. Yu, and X. Zeng, "Research on anti-corrosion property of rare earth inhibitor for X70 steel," *Journal of Rare Earths*, vol. 31, no. 7, pp. 734–740, 2013.

[52] D. Mohammedi, F. Ismail, R. Rehamnia, R. Bensalem, and O. Savadogo, "Corrosion behaviour of steel in the presence of rare earth salts: synergistic effect," *Corrosion Engineering, Science and Technology*, vol. 50, no. 8, pp. 633–638, 2015.

[53] J. Ostrowska-Czubenko and M. Gierszewska-Drużyńska, "Effect of ionic crosslinking on the water state in hydrogel chitosan membranes," *Carbohydrate Polymers*, vol. 77, no. 3, pp. 590–598, 2009.

[54] O. L. Riggs Jr., *Corrosion Inhibition*, C.C. Nathan, Houston, TX, USA, 2nd edition, 1973.

[55] M. A. Amin, M. A. Ahmed, H. A. Arida et al., "Monitoring corrosion and corrosion control of iron in HCl by non-ionic surfactants of the TRITON-X series – part III. Immersion time effects and theoretical studies," *Corrosion Science*, vol. 53, no. 5, pp. 1895–1909, 2011.

[56] M. S. Al-Otaibi, A. M. Al-Mayouf, M. Khan, A. A. Mousa, S. A. Al-Mazroa, and H. Z. Alkhathlan, "Corrosion inhibitory action of some plant extracts on the corrosion of mild steel in acidic media," *Arabian Journal of Chemistry*, vol. 7, no. 3, pp. 340–346, 2014.

[57] G. J. Brug, A. L. G. Van Den Eeden, M. Sluyters-Rehbach, and J. H. Sluyters, "The analysis of electrode impedances complicated by the presence of a constant phase element," *Journal of Electroanalytical Chemistry and Interfacial Electrochemistry*, vol. 176, no. 1-2, pp. 275–295, 1984.